Effects of site substitutions and concentration on upconversion luminescence of Er^{3+}-doped perovskite titanate

Yang Zhang, Jianhua Hao,* Chee Leung Mak and Xianhua Wei

Department of Applied Physics and Materials Research Centre, The Hong Kong Polytechnic University, Hong Kong
**apjhhao@polyu.edu.hk*

Abstract: Upconversion photoluminescence (PL) of Er^{3+}-doped $BaTiO_3$ (BTO) with perovskite ABO_3 structure is studied in terms of Er^{3+} substitutions for Ba (A-) and Ti (B-site) with different Er^{3+} doping concentrations. PL quenching with an increase Er^{3+} doping concentration is investigated based on the structural change and energy transfer of cross-relaxation process in BTO: Er, i.e. $^2H_{11/2} + {}^4I_{15/2} \rightarrow {}^4I_{9/2} + {}^4I_{13/2}$. Temperature dependence of the PL in BTO: Er is revealed, which is associated with phase transitions of BTO host. The results imply that the emission from substituted Er^{3+} ions may be used as a structural probe for the ferroelectric titanates.

OCIS codes: (190.7220) Upconversion; (160.5690) Rare-earth-doped materials; (160.2260) Ferroelectrics.

References and links

1. J. E. Daniels, W. Jo, J. Rödel, and J. L. Jones, "Electric-field-induced phase transformation at a lead-free morphotropic phase boundary: case study in a 93%$(Bi_{0.5}Na_{0.5})TiO_3$-7% $BaTiO_3$ piezoelectric ceramic," Appl. Phys. Lett. **95**(3), 032904 (2009).
2. S. Tinte, and M. G. Stachiotti, "Surface effects and ferroelectric phase transitions in $BaTiO_3$ ultrathin films," Phys. Rev. B **64**(23), 235403 (2001).
3. J. H. Hao, J. Gao, Z. Wang, and D. P. Yu, "Interface structure and phase of epitaxial $SrTiO_3$ (100) thin films grown directly on silicon," Appl. Phys. Lett. **87**(13), 131908 (2005).
4. R. A. Ganeev, M. Suzuki, M. Baba, M. Ichihara, and H. Kuroda, "Low- and high-order nonlinear optical properties of $BaTiO_3$ and $SrTiO_3$ nanoparticles," J. Opt. Soc. Am. B **25**(3), 325–333 (2008).
5. Y. X. Liu, W. A. Pisarski, S. J. Zeng, C. F. Xu, and Q. B. Yang, "Tri-color upconversion luminescence of Rare earth doped $BaTiO_3$ nanocrystals and lowered color separation," Opt. Express **17**(11), 9089–9098 (2009).
6. G. Schlaghechen, J. Gottmann, E. W. Kreutz, and R. Poprawe, "Pulsed laser deposition of Er: $BaTiO_3$ for planar waveguides," Appl. Phys., A Mater. Sci. Process. **79**, 1255–1257 (2004).
7. A. Polman, "Erbium as a probe of everything?" Physica B **300**(1-4), 78–90 (2001).
8. N. M. Samsuri, A. K. Zamzuri, M. H. Al-Mansoori, A. Ahmad, and M. A. Mahdi, "Brillouin-Erbium fiber laser with enhanced feedback coupling using common Erbium gain section," Opt. Express **16**(21), 16475–16480 (2008).
9. K. Takada, E. Chang, and D. M. Smyth, "Rare-earth addition to $BaTiO_3$," Adv. Ceram. **19**, 147–152 (1987).
10. T. D. Dunbar, W. L. Warren, B. A. Tuttle, C. A. Randall, and Y. Tsur, "Electron paramagnetic resonance investigations of lanthanide-doped barium titanate: dopant site occupancy," J. Phys. Chem. B **108**(3), 908–917 (2004).
11. M. T. Buscaglia, M. Viviani, V. Buscaglia, C. Bottino, and P. Nanni, "Incorporation of Er^{3+} into $BaTiO_3$," J. Am. Ceram. Soc. **85**(6), 1569–1575 (2002).
12. V. V. Mitic, Z. S. Nikolic, V. B. Pavlovic, V. Paunovic, M. Miljkovic, B. Jordovic, and L. Zivkovic, "Influence of rare-earth dopants on barium titanate ceramics microstructure and corresponding electrical properties," J. Am. Ceram. Soc. **93**(1), 132–137 (2010).
13. J. H. Hwang, and Y. H. Han, "Dielectric properties of erbium doped barium titanate," Jpn. J. Appl. Phys. **40**(Part 1, No. 2A), 676–679 (2001).
14. P. Z. Zhang, M. R. Shen, L. Fang, F. G. Zheng, X. L. Wu, J. C. Shen, and H. T. Chen, "Pr^{3+} photoluminescence in ferroelectric $(Ba_{0.77}Ca_{0.23})TiO_3$ ceramics: sensitive to polarization and phase transitions," Appl. Phys. Lett. **92**(22), 222908 (2008).
15. C. H. Wen, S. Y. Chu, Y. D. Juang, and C. K. Wen, "New phase transition of erbium-doped $KNbO_3$ polycrystalline," J. Cryst. Growth **280**(1-2), 179–184 (2005).
16. P. S. Dobal, and R. S. Katiyar, "Studies on ferroelectric perovskites and Bi-layered compounds using micro-Raman spectroscopy," J. Raman Spectrosc. **33**(6), 405–423 (2002).

#139664 - $15.00 USD Received 14 Dec 2010; revised 11 Jan 2011; accepted 11 Jan 2011; published 14 Jan 2011

17. J. H. Hao, S. A. Studenikin, and M. Cocivera, "Transient photoconductivity properties of tungsten oxide thin films prepared by spray pyrolysis," J. Appl. Phys. **90**(10), 5064–5069 (2001).
18. Z. L. Wang, H. L. W. Chan, H. L. Li, and J. H. Hao, "Highly efficient low-voltage cathodoluminescence of LaF_3:Ln^{3+} (Ln=Eu^{3+}, Ce^{3+}, Tb^{3+}) spherical particles," Appl. Phys. Lett. **93**(14), 141106 (2008).
19. C. E. Jiang, L. Fang, M. R. Shen, F. G. Zheng, and X. L. Wu, "Effects of Eu substituting positions and concentrations on luminescent, dielectric, and magnetic properties of $SrTiO_3$ ceramics," Appl. Phys. Lett. **94**(7), 071110 (2009).
20. E. Na, S. C. Choi, and U. Paik, "Temperature dependence of dielectric properties of rare earth element doped $BaTiO_3$," J. Ceram. Process. Res. **4**(4), 181–184 (2003).
21. M. Ishii, S. Komuro, T. Morikawa, and Y. Aoyagi, "Local structure analysis of optically active center in Er-doped ZnO thin film," J. Appl. Phys. **89**(7), 3679–3684 (2001).
22. Z. Zhou, T. Komori, T. Ayukawa, H. Yukawa, M. Morinaga, A. Koizumi, and Y. Takeda, "Li- and Er-codoped ZnO with enhanced 1.54 μm photoemission," Appl. Phys. Lett. **87**(9), 091109 (2005).

1. Introduction

Ferroelectric titanates such as $SrTiO_3$ and $BaTiO_3$ (BTO) with typical perovskite ABO_3 structure have been extensively studied due to their excellent dielectric, ferroelectric, and electro-optic properties [1–4]. Er^{3+} as an active ion has drawn broad attention to meet the request used for upconversion (UC) phosphors, planar waveguide and structural probe [5–8]. BTO doped with Er^{3+} ion has been extensively investigated in ferroelectricity, phase transitions and luminescence. It is noted that the radius of the Er^{3+} ion is intermediate between that of the Ba^{2+} ion and Ti^{4+} ion. Er^{3+} can occupy either A- or B-site depending on Ba/Ti ratio [9–12]. Dopant site location was found to play an important role in electrical properties of Er^{3+}-doped BTO [11–13]. It is known that crystal field caused by structure symmetry of the host materials would contribute to different perturbation in terms of the Er^{3+} inner shell transitions. Therefore, UC photoluminescence (PL) efficiency should be dependent on the excited-state dynamics of the Er^{3+} ions and their interactions with the host matrix [14,15]. The interactions are strongly influenced by the host and the dopant. Unfortunately, there is very limited knowledge about the influence of site substitution of Er^{3+}-doped BTO on its PL properties. Furthermore, BTO is a typical ferroelectric material that undergoes successive phase transitions under different temperatures. UC mechanism of substituting sites corresponding to different symmetry structures has not been investigated yet. In this work, BTO doped with different Er^{3+} substituting positions and concentrations were prepared. X-ray diffraction (XRD) and Raman spectra were used to reveal the lattice distortion with Er^{3+} doped. The PL spectra of Er^{3+}-doped BTO and the UC mechanism related to the structure and cross-relaxation (CR) were studied. The PL spectra as a function of measuring temperature were investigated in order to understand the relationship between phase transition and luminescent behavior.

2. Experiment

Er^{3+}-doped BTO powders with different site substitutions and concentrations were prepared by solid-state reaction method. Reagent grade $BaCO_3$, TiO_2, and Er_2O_3 powders were used as raw materials. The charge compensation could be compensated by barium and oxygen vacancy for the A- and B-site substitutions, respectively. Here the samples for A- and B-site substitutions are refered to $Ba_{1-3x/2}Er_xTiO_3$ (BTO: A) and $BaTi_{1-x}Er_xO_{3-x/2}$ (BTO: B), respectively. Based on the above formulas, the starting powders with designed stoichiometric quantities were ball milled for 24 h, then dried and calcinated at 1100 °C for 8 h in air to generate the Er^{3+}-doped BTO powders.

The crystal structure of the samples was examined by a Bruker D8 Advance X-ray diffractometer (XRD). Raman spectra were measured using a Horiba Jobin Yvon HR800 Raman spectrometer with a 488 nm laser excitation source. The PL spectra were recorded using an Edinburgh FLSP920 spectrophotometer under the excitation of a 980 nm laser diode. The fluorescence lifetimes for Er^{3+} were recorded at 552 nm with a μF900H micro-second flashlamp (λ_{ex} = 488 nm) as the excitation sources. The temperature-dependent PL spectra were carried out in the temperature range of 15-300 K.

#139664 - $15.00 USD Received 14 Dec 2010; revised 11 Jan 2011; accepted 11 Jan 2011; published 14 Jan 2011

3. Results and discussion

Figure 1 shows the XRD patterns of Er^{3+}-doped BTO with different site substitutions and concentrations. The characteristic diffraction peaks of tetragonal BTO phase without secondary impurity phases were observed. The result implied that Er^{3+} ions were doped efficiently into BTO host. A comparison of these XRD patterns with various Er^{3+} doping shows the broaden diffraction peaks for samples with higher Er^{3+} doping concentrations as shown in Fig. 1. It suggests that the doping with higher Er^{3+} concentrations may lead to the worse crystalline of doped BTO. In addition, compared with pure BTO, there are minor shifts of the diffraction peak (111) for the Er^{3+} doped samples as seen in the inset of Fig. 1. It means that the lattice constant of Er^{3+}-doped BTO shrinks or expands in the case of Er^{3+} occupying A- or B-site, respectively [12,19].

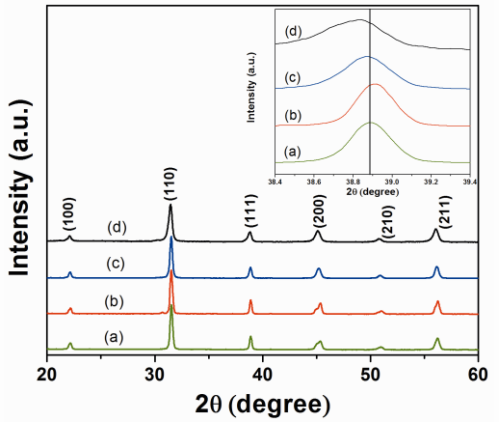

Fig. 1. XRD patterns of the pure BTO and Er^{3+}-doped BTO with different site substitutions and concentrations: (a) pure, (b) x = 3 mol% with A-site substitution, (c) x = 3 mol% with B-site substitution and (d) x = 5 mol% with B-site substitution. The inset shows the enlarged (111) peak.

Figure 2 gives the Raman spectra of Er^{3+}-doped BTO and pure BTO at room temperature. BTO exhibits tetragonal structure belonging to the space group C_{4v} symmetry. All of the features observed in the tetragonal phase have been reported in the literature [16]. The peak observed at 305 cm^{-1} corresponds to the $E(TO_2)$ phonon mode of tetragonal BTO. The $A_1(TO_1)$, $A_1(TO_2)$, $A_1(TO_3)$ and $A_1(LO_3)$ modes were observed at about 180, 270, 516 and 720 cm^{-1}, respectively. Raman spectra obtained from Er^{3+}-doped BTO did not show any remarkable wavelength shift. It can also be seen that all Raman modes become weaker and broader with an increase in Er^{3+} concentration. It indicates the higher Er^{3+} concentration results in the worse crystallinity, which is consistent with the XRD results.

#139664 - $15.00 USD Received 14 Dec 2010; revised 11 Jan 2011; accepted 11 Jan 2011; published 14 Jan 2011

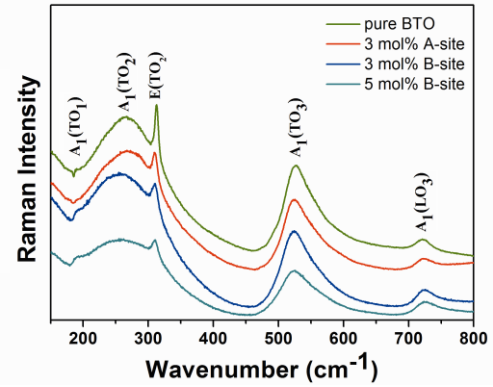

Fig. 2. Raman spectra of the pure BTO and Er^{3+}-doped BTO with different site substitutions and concentrations.

Figure 3 shows the PL spectra of BTO doped with different Er^{3+} ion concentrations and site substitutions measured at room temperature. The typical UC emission consists of two strong green bands located at 523 and 552 nm corresponding to $^2H_{11/2}/^4S_{3/2} \rightarrow ^4I_{15/2}$ transitions, and a weak red emission band at 656 nm ascribed to $^4F_{9/2} \rightarrow ^4I_{15/2}$ transition of the Er^{3+} ion, respectively. Obvious Stark-splitting can be observed in all samples. Note that with an increase in Er^{3+} doping concentration (0.5-5 mol% for BTO: B), the emission intensity reaches a maximum value at 1 mol%, and then decreases with an increase in doping concentration. There are two reasons responsible for this observation. Structural analysis based on XRD and Raman spectra has revealed that worse crystalline occurs in BTO: Er with increasing Er^{3+} content. Worse crystalline phase corresponds to higher defect density of the materials. Both subband gap defect levels and impurity atoms in the grain boundaries could participate in the relaxation process and change the probability of radiative recombination [17,18]. On the other hand, an increased dopant concentration could also enhance CR process with remarkable decrease UC emission as shown in Fig. 4. Under the excitation of 980 nm, through excited state absorption (ESA) or energy transfer (ET) process, Er^{3+} ion can populates the $^4F_{7/2}$ level. Subsequently, the Er^{3+} ion then relaxes nonradiatively to the $^2H_{11/2}$ and $^4S_{3/2}$ levels by multiphonon relaxation, from which the green $^2H_{11/2}/^4S_{3/2} \rightarrow ^4I_{15/2}$ emissions occur. As shown in Fig. 3, red UC emissions from the $^4F_{9/2}$ state are weak, since the $^4F_{9/2}$ state has a relatively large energy separation below the $^4S_{3/2}$ state, compared with the phonon energy of the BTO lattice. Moreover, we calculated the intensity of green-to-red ratio (I_{523nm}/I_{656nm}) for the BTO: B sample as shown in the inset of Fig. 3. It can be seen that the ratio (I_{523nm}/I_{656nm}) is 23.4, 24.2, 5.7, and 1.8 for 0.5, 1, 3, and 5 mol% B-site Er^{3+}-doped BTO, respectively. The result can be understood based on the CR process shown in Fig. 4. Higher Er^{3+} concentration contributing to a shorter distance between ions results in an enhanced ET probability of the CR process, i.e. $^2H_{11/2} + {}^4I_{15/2} \rightarrow {}^4I_{9/2} + {}^4I_{13/2}$. Hence, the Er^{3+} ions at $^4I_{13/2}$ state through ESA populate the $^4F_{9/2}$ state. This enhanced population of the $^4F_{9/2}$ state primarily enhances the intensity of the red emission.

#139664 - $15.00 USD Received 14 Dec 2010; revised 11 Jan 2011; accepted 11 Jan 2011; published 14 Jan 2011

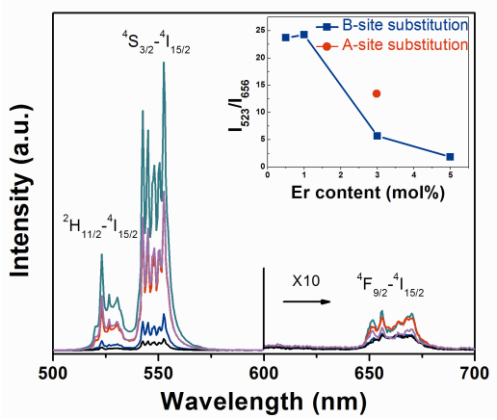

Fig. 3. The PL spectra of BTO: A with x = 3 mol% (red) and BTO: B with x = 0.5 mol% (magenta), 1 mol% (cyan), 3 mol% (blue) and 5 mol% (black). The inset shows the green-to-red ratio (I_{523nm}/I_{656nm}) vs dopant concentration.

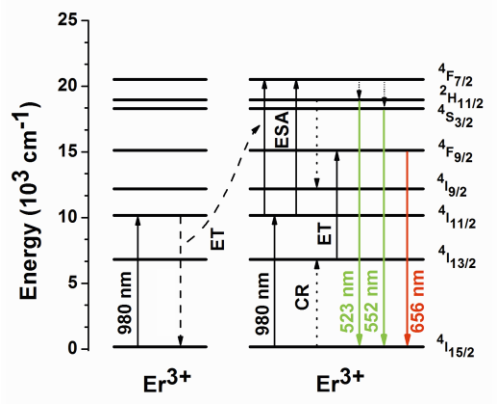

Fig. 4. Schematic diagram for the UC mechanism of Er^{3+} ions under 980 nm excitation.

The PL spectra of BTO with 3 mol% Er^{3+} ion doped for A- and B-site substitutions are also presented in Fig. 3. The PL intensity differs for different site substitutions, but there is no obvious shift of the emission peaks. These results indicate that the crystal field surrounding the erbium ions can change the relative radiative probability of the transitions from the excited state to the eight Stark components of the $^4I_{15/2}$ ground state. The PL intensity of A-site doped sample is much stronger than that of B-site doped BTO. Compared with that of A-site doped sample, the decrease in PL intensity for B-site substitution Er^{3+}-doped BTO may be affected by oxygen vacancies when Er^{3+} as an acceptor type impurity replaces Ti site, leading to an oxygen-deficient nonstoichiometry [13,19]. Compared the fluorescence lifetimes for two samples at 552 nm corresponding to $^4S_{3/2} \rightarrow {}^4I_{15/2}$ transition, the double exponential fitting results for A- and B-site doped samples are 132 and 52 ms, respectively. The decrease of lifetime of B-site substituted sample could be ascribed to the introduction of oxygen vacancies. We speculate that these oxygen vacancies would induce mew energy levels, which promote nonradiative energy transfer.

#139664 - $15.00 USD Received 14 Dec 2010; revised 11 Jan 2011; accepted 11 Jan 2011; published 14 Jan 2011

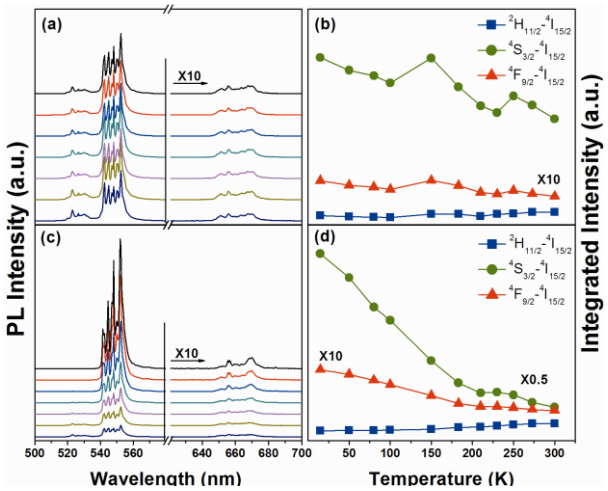

Fig. 5. (a) and (c) show the PL spectra of Er^{3+}-doped BTO (x = 3 mol%) with different substitutions at different temperatures 15 K (black), 50 K (red), 100 K (blue), 150 K (cyan), 183 K (magenta), 250 K (yellow) and 300 K (navy). (b) and (d) show the corresponding integrated intensity of three emissions at different temperatures. (a) and (b) for A-site substitution, (c) and (d) for B-site substitution.

It is well-known that BTO undergoes successive phase transitions. PL evolution of the samples has been evaluated as a function of temperatures between 15 and 300 K as shown in Fig. 5. It shows that the PL response of Er^{3+} ions to the structural changes occurring during phase transition is related to their site location in the BTO host. Figure 5(a) shows the temperature dependence of the PL intensity for the case of A-site substitution. It is known that pure BTO crystal undergoes ferroelectric phase transitions at 278 and 183 K. Rare-earth doping has slight influence on the phase transition temperature of BTO [20]. As presented in Fig. 5(b), the abnormal jump in PL intensity across the vicinity of 150 K and 250 K may be related to the crystal field changes around Er^{3+} ions induced by the phase transition. For the B-site substitution, Fig. 5(c) illustrates that the UC emission from $^2H_{11/2}$ is strongly suppressed, while the emission from $^4S_{3/2}$ increases remarkably. The $^2H_{11/2}$ state is thermally quenched to $^4S_{3/2}$ state and subsequently contributed to the enhanced population of $^4S_{3/2}$ state with decreasing temperature. Apart from the thermal quenching, the phenomenon is also relative to the crystal field. The crystal field formed by the octahedral oxygen ions with a lower symmetry than O_h is more suitable for the Er intra-4f transitions [21,22]. Therefore, Er^{3+} located B-site with lower symmetry due to phase transition facilitates the UC emissions. An increase in red emission $^4F_{9/2} \rightarrow {}^4I_{15/2}$ with lower symmetry occurs as evidenced in Fig. 5(d). The characteristics imply that the emission from substituted Er^{3+} ions can be used as a structural probe for the BTO.

4. Conclusions

In conclusion, PL quenching of Er^{3+}-doped BTO is due to the worse crystalline and cross-relaxation with an increase in Er^{3+} doping concentration. Phase transition results in the increase of PL spectra of A-site doped BTO across the phase transition temperature. For the case of B-site substitution, $^4S_{3/2} \rightarrow {}^4I_{15/2}$ emissions are strongly enhanced due to thermal quenching and lower symmetry induced by phase transition.

Acknowledgments

The work was supported by grants from the Research Grants Council of Hong Kong (GRF No. PolyU500910) and Hong Kong Polytechnic University (No. A-PH89).

#139664 - $15.00 USD Received 14 Dec 2010; revised 11 Jan 2011; accepted 11 Jan 2011; published 14 Jan 2011